Stereodynamics of *N*-Ethyl-*N*-methyl-2-aminopropane. ^1H and $^{13}C\{^1H\}$ DNMR Studies. Molecular Mechanics Calculations

Jay H. Brown and C. Hackett Bushweller*

Department of Chemistry, University of Vermont, Burlington, Vermont 05405-0125

Received: June 22, 1994; In Final Form: August 22, 1994[⊗]

N-Ethyl-*N*-methyl-2-aminopropane (**EMAP**) is one of the simplest tertiary aliphatic amines that has a chiral center at nitrogen. Racemization occurs by inversion−rotation at the pyramidal nitrogen. For each **EMAP** enantiomer, additional conformational interconversions occur via isolated rotation about carbon−nitrogen bonds. The ^1H and $^{13}C\{^1H\}$ dynamic NMR (DNMR) spectra of **EMAP** and a selectively deuterated derivative decoalesce into four subspectra at 95 K. The spectrum at 95 K is best rationalized in terms of five equilibrium conformations present at concentrations high enough to be NMR-detectable including two conformations that interchange rapidly even at 95 K. A two-letter designation is used to name the various conformations. The first letter defines the orientation of the ethyl methyl group (**G** denotes gauche to the lone pair and to the *N*-methyl group; **G′** denotes gauche to the lone pair and to the isopropyl group; **A** denotes anti to the lone pair). The second letter defines the orientation of the isopropyl methine proton (**G** denotes gauche to the lone pair and to the *N*-methyl group; **G′** denotes gauche to the lone pair and to the ethyl group; **A** denotes anti to the lone pair). The major subspectrum at 95 K is assigned to a family of **G′G′** and **GG′** conformations (59%) that interconvert rapidly at 95 K. The other three subspectra are assigned to the **GG** (34%), **AA** (5%), and **GA** (2%) conformations. Simulations of the DNMR spectra reveal a barrier to inversion−rotation at nitrogen ($\Delta G^{\ddagger} = 7.5$ kcal/mol at 160 K) that is higher than the barriers for a number of observable isolated rotations about the N−CH_2 and N−CH bonds ($\Delta G^{\ddagger} = 4.7$−6.4 kcal/mol). A 5000-point optimized energy surface computed as a function of two dihedral angles by using Allinger's MM2(87) computer program, MM2(87) energy calculations for *all* the optimized equilibrium conformations of **EMAP**, and MM2(87)-calculated isolated rotation barriers show excellent agreement with the DNMR data.

Introduction

Two types of internal motion are important in simple tertiary aliphatic amines. One process is isolated rotation about single bonds, and the other is inversion at the pyramidal nitrogen.[1,2] Pyramidal inversion is a complex process that involves not only inversion at the pyramidal nitrogen but also requires concomitant rotation about carbon−nitrogen bonds.[1,2] The process is best characterized as *inversion−rotation*. Barriers to isolated rotation about single bonds and conformational preferences for several simple amines including methylamine,[3] dimethylamine,[3] trimethylamine,[3] ethylamine,[4] isopropylamine,[5] ethylmethylamine,[6] and dimethylethylamine[7] have been measured by using microwave, infrared, and Raman spectroscopy and calculated by using molecular orbital theory. Microwave and infrared spectroscopies in conjunction with appropriate potential functions, have been used to measure inversion barriers in ammonia,[8] methylamine,[9] dimethylamine,[10] and trimethylamine.[11]

The dynamic NMR (DNMR) method in conjunction with molecular mechanics calculations has proven to be an effective approach to studies of the stereodynamics of several other unencumbered trialkylamines including diethylmethylamine,[12] triethylamine,[12] dibenzylmethylamine,[1] tribenzylamine,[13] 2-butylethylmethylamine,[14] and isopropyldimethylamine.[15]

N-Ethyl-*N*-methyl-2-aminopropane (**EMAP**) is one of the simplest tertiary aliphatic amines that has a chiral center at nitrogen. Racemization occurs by inversion−rotation at the pyramidal nitrogen. For each **EMAP** enantiomer, additional conformational interconversions occur via isolated rotation about carbon−nitrogen bonds. Isolated rotation about carbon−nitrogen single bonds and inversion−rotation at nitrogen were first observed in the same molecule by examining the ^1H DNMR spectra of a deuterated derivative of **EMAP** at a low NMR observation frequency (60 MHz).[16] In this study, important aspects of **EMAP** stereodynamics were obscured by the low ^1H NMR observation frequency.[16] Minor conformations were not detected. As a result, the kinetics of conformational exchange derived from theoretical DNMR line shape simulations were compromised. In this paper, we report a thorough reinvestigation of the stereodynamics of **EMAP** by using ^1H (270 MHz) and $^{13}C\{^1H\}$ (62.9 MHz) DNMR spectroscopy complemented by extensive molecular mechanics calculations. The enhanced chemical shift dispersion associated with a higher ^1H NMR observation frequency and the inherently greater chemical shift dispersion of ^{13}C NMR spectra provide significantly improved experimental data regarding the stereodynamics of **EMAP**. The DNMR spectra show multiple decoalescence phenomena due to a relatively high barrier to inversion and lower barriers associated with isolated rotation processes. Complete line shape simulations reveal that the experimental spectrum results from the superposition of four unequally populated subspectra. The spectrum at 95 K is best rationalized in terms of five equilibrium conformations present at concentrations high enough to be NMR-detectable, including two conformations that interchange rapidly even at 95 K. Molecular mechanics calculations including a 5000-point energy contour computation are in excellent agreement with the NMR data.[17] The NMR studies in conjunction with the molecular mechanics calculations allow elucidation of a comprehensive picture of **EMAP** stereodynamics.

DNMR Studies

The $^{13}C\{^1H\}$ NMR spectrum (62.9 MHz) of **EMAP** (3% v/v in $CBrF_3$) at 200 K shows five singlets at δ 12.87 (methyl carbon

[⊗] Abstract published in *Advance ACS Abstracts,* October 1, 1994.

0022-3654/94/2098-11411$04.50/0

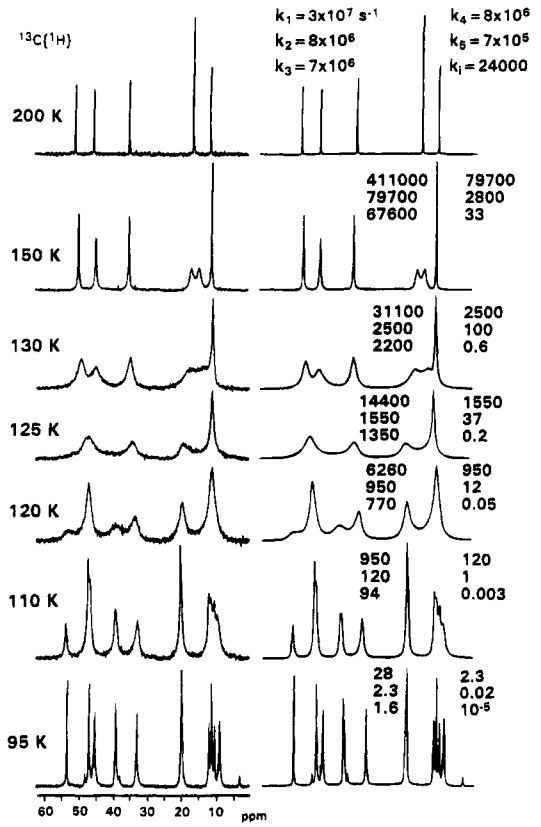

Figure 1. Experimental $^{13}C\{^1H\}$ DNMR spectra (62.898 MHz) of *N*-ethyl-*N*-methyl-2-aminopropane (**EMAP**; 3% v/v in $CBrF_3$) in the left column and theoretical simulations in the right column. The rate constants are defined in Scheme 1.

on ethyl group), δ 17.8 (methyl carbons on isopropyl group), δ 36.88 (*N*-methyl carbon), δ 47.69 (methylene carbon), and δ 53.26 (methine carbon) as shown in Figure 1. At 150 K, the signal due to the methyl carbons on the isopropyl group decoalesces in response to slowing *inversion–rotation* on the NMR chemical exchange time scale.[1,2,12–16] At 150 K, all other resonances remain sharp. In all the stable equilibrium conformations of **EMAP**, the geometry about the chiral nitrogen is pyramidal. The methyl carbons on the isopropyl group are diastereotopic. Both inversion–rotation at the pyramidal nitrogen and isolated 3-fold rotation about carbon–nitrogen bonds (i.e., rotation without concomitant inversion) are required to effect a complete mutual interchange of the molecular environments of the isopropyl methyl carbons and to effect a complete mutual interchange of the chemical shifts of these carbons.[1,2,12–16] Rapid isolated rotation about carbon–nitrogen bonds by itself is not sufficient to achieve such a mutual interchange. Thus, if inversion–rotation is slow on the NMR chemical exchange time scale while all isolated rotations remain fast, the methyl carbons on the isopropyl group will show two different NMR chemical shifts reflecting the diastereotopic character of those carbon atoms. At 150 K, decoalescence of the isopropyl methyls resonance into two peaks of equal intensity is consistent with slow inversion–rotation while all isolated rotations remain fast.[1,2,12–16] Below 150 K, a complex decoalescence occurs due to slowing isolated rotation about carbon–nitrogen bonds. At 95 K, essentially slow exchange conditions are reached (Figure 1).

By using computer program DNMR6, theoretical simulations of the $^{13}C\{^1H\}$ DNMR spectra of **EMAP** allowed identification of subspectra due to equilibrium conformations that are present at concentrations high enough to be NMR-detectable, elucidation of the preferred pathways for magnetization exchange and,

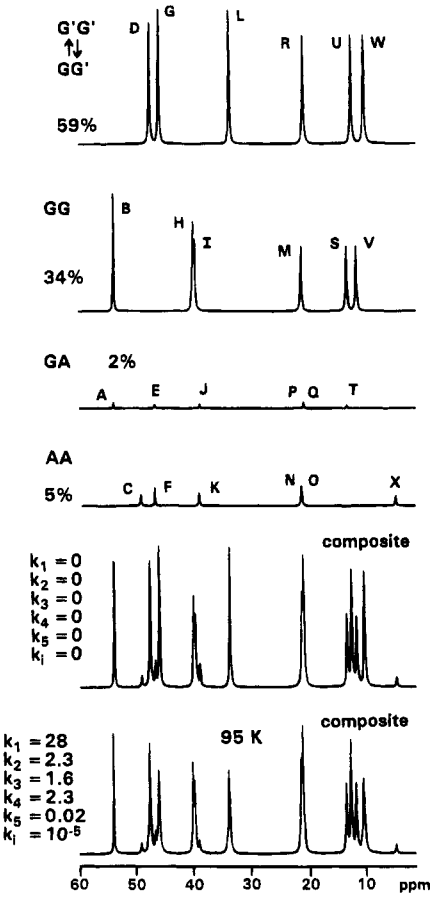

Figure 2. Decomposition of the theoretical simulation of the $^{13}C\{^1H\}$ NMR spectrum of *N*-ethyl-*N*-methyl-2-aminopropane (**EMAP**) at 95 K. The upper four subspectra are assigned to specific conformations as indicated. The top subspectrum is due to the rapidly exchanging family of **G'G'** and **GG'** conformations. The upper composite spectrum is calculated with all rate constants equal to zero. The bottom composite spectrum is computed by using the rate constants necessary to obtain an accurate fit of the experimental spectrum.

TABLE 1: ^{13}C NMR Chemical Shifts for the Stable, Equilibrium Conformations of EMAP[a]

	conformations[c]			
carbon(s)[b]	**G'G'** ⇌ **GG'** (59%)	**GG** (34%)	**GA** (2%)	**AA** (5%)
$CH(*CH_3)_2$	δ_R 21.62[d]	δ_M 21.97[d]	δ_P 21.62[d]	δ_N 21.87[d]
	δ_W 10.71[e]	δ_V 12.08[e]	δ_Q 21.62[d]	δ_O 21.87[d]
$*CH(CH_3)_2$	δ_G 47.53	δ_B 55.72	δ_A 55.80	δ_F 48.22
CH_2*CH_3	δ_U 12.99[d]	δ_S 13.83[d]	δ_T 13.83[d]	δ_X 5.01[e]
$*CH_2CH_3$	δ_D 49.21	δ_I 41.10	δ_E 48.33	δ_C 50.71
NCH_3	δ_L 34.98	δ_H 41.41	δ_J 40.30	δ_K 40.30

[a] 95 K in $CBrF_3$. [b] Indicated by an asterisk. [c] See Scheme 1. See Figure 2 for a spectral decomposition at 95 K. [d] Gauche to nitrogen lone pair. [e] Anti to nitrogen lone pair.

ultimately, the preferred pathways for conformational exchange.[18] The spectra at 95 K and above could be simulated accurately only by invoking the presence of four subspectra. The four separate subspectra are illustrated as the upper four spectra in Figure 2. The ^{13}C NMR chemical shifts for all resonances in each subspectrum are compiled in Table 1. Superposition of the properly weighted upper four subspectra produces the composite spectrum under conditions of no exchange of magnetization (second spectrum from bottom in Figure 2). At 95 K, one magnetization exchange occurs at a rate fast enough to differentially broaden certain signals and this exchange must be incorporated into calculation of the composite theoretical spectrum (bottom spectrum of Figure 2) that gives an accurate simulation of the experimental spectrum

TABLE 2: Barriers to Isolated Rotation about Carbon–Nitrogen Bonds in EMAP Measured by $^{13}C\{^1H\}$ DNMR Spectroscopy

substituent	magnetization transfer[a]	rate constant,[b] s^{-1}	conformational exchange[b]	$\Delta G^{\ddagger}$ (temp), kcal/mol
$CH(CH_3)_2$	RGW to PAQ (or QAP)	k_1	**G'G'/GG'** to **GA**	4.7 ± 0.1 (95 K)
	RGW to NFO	k_2	**G'G'/GG'** to **AA**	5.2 ± 0.1 (110 K)
	VBM to PAQ (or QAP)	k_3	**GG** to **GA**	5.2 ± 0.1 (110 K)
	PAQ (or QAP) to NFO	k_4	**GA** to **AA**	5.2 ± 0.1 (110 K)
	RGW to VBM	k_5	**G'G'/GG'** to **GG**	6.2 ± 0.4 (130 K)
CH_2CH_3	DU to ET	k_1	**G'G'/GG'** to **GA**	4.7 ± 0.1 (95 K)
	DU to CX	k_2	**G'G'/GG'** to **AA**	5.2 ± 0.1 (110 K)
	IS to ET	k_3	**GG** to **GA**	5.2 ± 0.1 (110 K)
	ET to CX	k_4	**GA** to **AA**	5.2 ± 0.1 (110 K)
	DU to IS	k_5	**G'G'/GG'** to **GG**	6.2 ± 0.4 (130 K)
NCH_3	L to J	k_1	**G'G'/GG'** to **GA**	4.7 ± 0.1 (95 K)
	L to K	k_2	**G'G'/GG'** to **AA**	5.2 ± 0.1 (110 K)
	H to J	k_3	**GG** to **GA**	5.2 ± 0.1 (110 K)
	J to K	k_4	**GA** to **AA**	5.2 ± 0.1 (110 K)
	L to H	k_5	**G'G'/GG'** to **GG**	6.2 ± 0.4 (130 K)

[a] See Table 1 and Figures 1 and 2. [b] See Scheme 1.

at 95 K. Individual resonances for three subspectra with populations of 59%, 34%, and 5% are resolved at 95 K (Figure 2, Table 1). The signals associated with the fourth subspectrum (2%) overlap those of other subspectra (Figure 2, Table 1). The presence of this subspectrum was inferred from theoretical DNMR line shape simulations (*vide infra*). In the regions of intermediate and fast exchange, the DNMR line shape will be determined by those rates of magnetization exchange that are associated with the minimum energy or preferred pathways for conformational interconversion. Therefore, the approach used in simulating the DNMR spectra was to start at 95 K and, as the sample temperature increased, to turn on only those magnetization transfers (and the associated back transfers) that are necessary and sufficient to achieve an accurate complete line shape simulation (Figure 1). The magnetization transfers necessary and sufficient to achieve accurate complete DNMR line shape simulations from 95 K to 130 K are compiled in Table 2. All of these processes involve isolated rotation about *N*-ethyl and *N*-isopropyl bonds while inversion–rotation remains slow. Above 130 K, it is necessary to turn on random exchange among all the signals due to the methyl carbon atoms on the isopropyl group. This reflects the onset of inversion–rotation (k_i in Figure 1). While invoking magnetization transfers associated with rate constants k_1-k_5 (Table 2) was sufficient to generate accurate theoretical simulations of the experimental spectra up to 130 K (Figure 1), incorporating relatively low rates of BMV to FNO (isopropyl group; see Table 1), IS to CX (ethyl group) and H to K (*N*-methyl) exchanges (k_6) also gave acceptable fits. While it is not possible to obtain an accurate measure of k_6, it is clear that it is about ten times smaller than k_1-k_4 and comparable to k_5 at 110 K. At 95 K, one exchange (k_1 and its back reaction; Table 2; Figures 1 and 2) occurs at a rate fast enough to differentially broaden certain signals.

As stated above, the resonances due to one minor subspectrum (2% at 95 K; Table 1; Figure 2) are not resolved. The presence of this subspectrum was inferred from the line shape simulations. To achieve accurate, internally consistent theoretical line shape simulations, this subspectrum must be incorporated into the calculations. For example, accurate simulation of the spectrum at 110 K required a subspectral population of 5%. The spectrum at 110 K is especially sensitive to the existence of this subspectrum. In theoretical spectrum (a) of Figure 3, the minor subspectrum has been removed. Except for magnetization exchanges that involve the deleted minor subspectrum, all other exchanges remain the same as those indicated in Figure 1 with $k_6 = 1$. The discrepancy between the experimental and theoretical line shapes is clear. Attempts to improve the line shape by varying the rates were unsuccessful. For example,

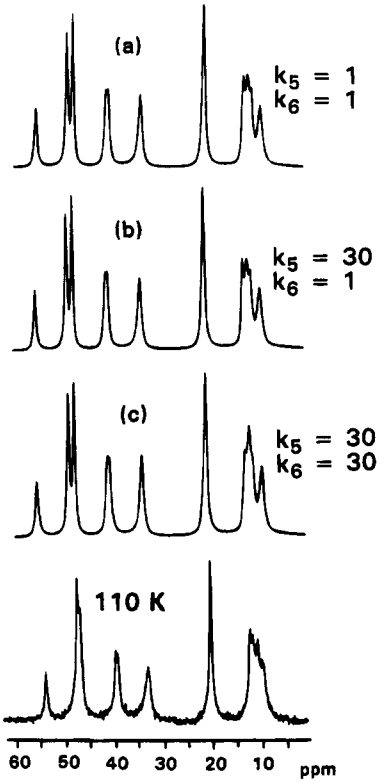

Figure 3. (a–c) Attempts at theoretical simulations of the $^{13}C\{^1H\}$ DNMR spectrum of **EMAP** at 110 K computed without the inferred minor subspectrum. Bottom: experimental spectrum at 110 K. Accurate simulation requires 5% of inferred minor subspectrum at 110 K (see Figure 1).

spectra (b) and (c) in Figure 3 show that increasing k_5 or k_6 does not improve the agreement between the theoretical and experimental line shapes. After an exhaustive, systematic search, we could find no internally consistent combinations of exchange rates that would give accurate theoretical line shapes without the minor subspectrum.

To provide additional data regarding the stereodynamics of **EMAP**, we examined the ^1H DNMR spectra (270 MHz) of $(CH_3)_2CDN(CD_3)CH_2CD_3$ (**EMAP-d_7**; 3% v/v in $CBrF_3$). For **EMAP-d_7**, certain ^1H NMR signals and all vicinal proton–proton spin–spin coupling are removed resulting in useful spectral simplification. At 200 K, the spectrum of **EMAP-d_7** shows two singlets at δ 0.98 [$CD(CH_3)_2$] and δ 2.37 [CH_2CD_3] as shown in Figure 4. At 148 K, the signal due to the methylene protons is decoalesed into two differentially broadened doublets

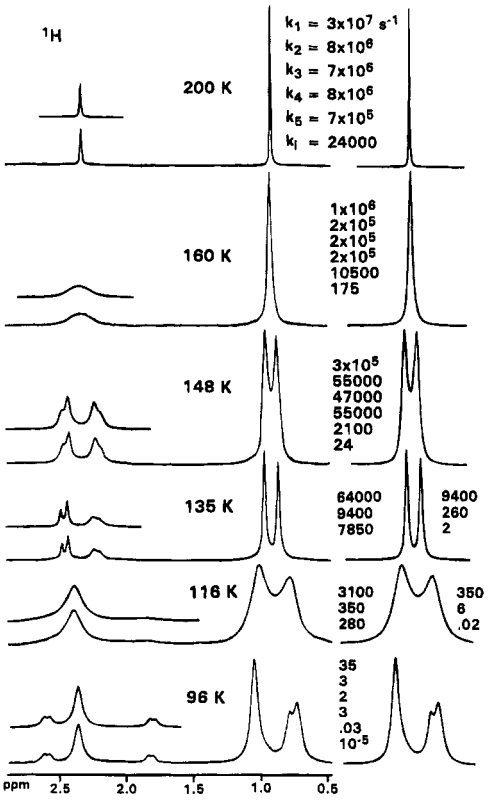

Figure 4. Experimental ^{1}H DNMR spectra (270 MHz) of $(CH_3)_2CDN(CD_3)CH_2CD_3$ (**EMAP-d_7**; 3% v/v in $CBrF_3$) and theoretical simulations above the CD_3CH_2 and to the right of the $CD(CH_3)_2$ subspectra. The rate constants are defined in Scheme 1.

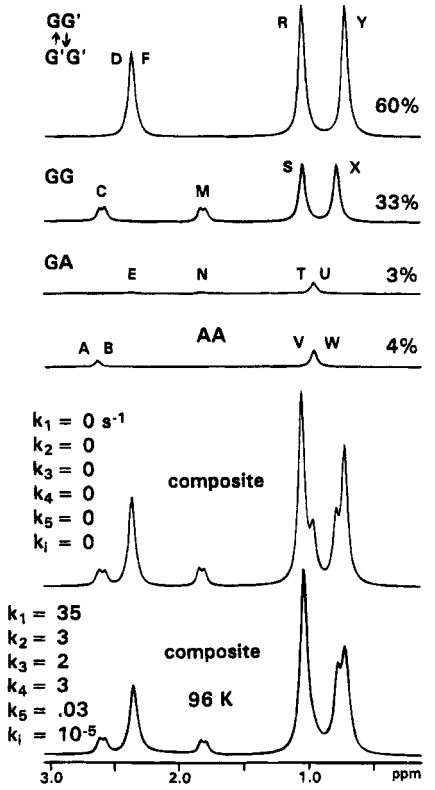

Figure 5. Decomposition of the theoretical simulation of the ^{1}H NMR spectrum (270 MHz) of $(CH_3)_2CDN(CD_3)CH_2CD_3$ (**EMAP-d_7**) at 96 K. The format for presentation of the subspectra and composite spectra is identical to that in Figure 2.

and the resonance due to the isopropyl methyl groups is decoalesced into two singlets. This is consistent with slow nitrogen inversion on the NMR chemical exchange time scale while isolated rotation about carbon–nitrogen and carbon–carbon bonds remains significantly faster at 148 K (*vide supra*).[1,2,12–16] The asymmetric shape of the methylene protons resonances at 148 K is due to the onset of slowing isolated rotation about carbon–nitrogen bonds. Below 148 K, a complex decoalescence occurs due to slowing isolated rotation about carbon–nitrogen bonds. At 96 K, an accurate complete line shape simulation requires the use of four unequally populated subspectra.[18] The four separate subspectra are illustrated as the upper four spectra in Figure 5. The ^{1}H NMR chemical shifts for all resonances in each subspectrum are compiled in Table 3. Resonances due to the two major subspectra are clearly resolved especially for the methylene protons (see CM and DF spectra in Figure 5). The AB spectrum due to one minor species (4%; Figure 5) is superimposed on the low-field component of the C doublet of the CM spectrum (33%), and its presence can be verified by simulation. For the subspectrum that has a 3% relative intensity (Figure 5), the superimposed methyl chemical shifts at δ_T 1.07 and δ_U 1.07 are required for an accurate fit of the total line shape under conditions of slow and intermediate rates of exchange and are located with reasonable accuracy. Location of the methylene protons chemical shifts at δ_E 2.41 and δ_N 1.88 is more problematic. However, in simulating the exchange-broadened spectra, it was necessary to employ a relatively large $\Delta\delta_{EN}$ value in order to achieve accurate spectral fits. Superposition of the properly weighted subspectra produces the composite spectrum under conditions of no exchange of magnetization (second spectrum from the bottom in Figure 5). Consistent with the $^{13}C\{^1H\}$ DNMR spectra, one magnetization exchange (k_1 and its back reaction) occurs at a rate fast enough at 96 K to affect the DNMR line shape. This rate must be incorporated into calculation of the composite theoretical spectrum of **EMAP-d_7** (bottom spectrum of Figure 5) that gives an accurate fit of the experimental spectrum at 96 K. The magnetization exchanges that are necessary and sufficient to achieve accurate theoretical line shape simulations from 96 to 135 K are compiled in Table 4. The exchange itineraries and rates agree with those derived from the $^{13}C\{^1H\}$ DNMR spectra.

The ^{13}C NMR spectrum at 95 K can be used in conjunction with the ^{1}H NMR spectrum at 96 K to identify all the **EMAP** equilibrium conformations that are present at concentrations high enough to be NMR-detectable. A two-letter designation will be used to name the various conformations. The first letter defines the orientation of the ethyl methyl group (**G** denotes gauche to the lone pair and to the *N*-methyl group; **G′** denotes

TABLE 3: ^{1}H NMR Parameters for the Stable, Equilibrium Conformations of EMAP-d_7[a]

	conformations[b]			
substituent	**G′G′ ⇌ GG′** (60%)	**GG** (33%)	**GA** (3%)	**AA** (4%)
$CD(CH_3)_2$	δ_R 1.12[c]	δ_S 1.12[c]	δ_T 1.07[c]	δ_V 1.07[c]
	δ_Y 0.80[d]	δ_X 0.86[d]	δ_U 1.07[c]	δ_W 1.07[c]
CH_2CD_3	δ_D 2.43	δ_C 2.64	δ_E 2.41	δ_A 2.68
	δ_F 2.40	δ_M 1.88	δ_N 1.88	δ_B 2.68
	$^2J_{DF} = -11.5$[e]	$^2J_{CM} = -11.5$[e]	$^2J_{EN} = -11.5$[e]	$^2J_{AB} = -11.5$[e]

[a] 96 K in $CBrF_3$. [b] See Scheme 1. See Figure 4 for a spectral decomposition at 96 K. [c] Gauche to the lone pair. [d] Anti to the lone pair. [e] Hertz.

TABLE 4: Barriers to Isolated Rotation about Carbon−Nitrogen Bonds in EMAP-d_7 Measured by ^{1}H DNMR Spectroscopy

substituent	magnetization transfer[a]	rate constant,[b] s^{-1}	conformational exchange[b]	$\Delta G^{\ddagger}$ (temp), kcal/mol
$CD(CH_3)_2$	RY to TU (or UT)	k_1	**G'G'/GG'** to **GA**	5.0 ± 0.1 (112 K)
	RY to VW (or WV)	k_2	**G'G'/GG'** to **AA**	5.2 ± 0.1 (114 K)
	SX to TU (or UT)	k_3	**GG** to **GA**	5.3 ± 0.1 (114 K)
	TU to VW (or WV)	k_4	**GA** to **AA**	5.2 ± 0.1 (114 K)
	RY to XS	k_5	**G'G'/GG'** to **GG**	6.4 ± 0.4 (125 K)
CH_2CD_3	DF to EN	k_1	**G'G'/GG'** to **GA**	5.0 ± 0.3 (112 K)
	DF to AB (or BA)	k_2	**G'G'/GG'** to **AA**	5.2 ± 0.1 (114 K)
	CM to EN	k_3	**GG** to **AA**	5.3 ± 0.1 (114 K)
	EN to AB (or BA)	k_4	**GA** to **AA**	5.2 ± 0.1 (114 K)
	DF to CM	k_5	**G'G'/GG'** to **GG**	6.4 ± 0.4 (125 K)

[a] See Table 2 and Figures 3 and 4. [b] See Scheme 1.

gauche to the lone pair and to the isopropyl group; **A** denotes anti to the lone pair). The second letter defines the orientation of the isopropyl methine proton (**G** denotes gauche to the lone pair and to the *N*-methyl group; **G'** denotes gauche to the lone pair and to the ethyl group; **A** denotes anti to the lone pair).

The major ^{13}C NMR subspectrum (59%; Figure 2, Table 1) shows two well-separated isopropyl methyl resonances at δ_R 21.62 and δ_W 10.71. On the basis of well-established chemical shift trends, the signal at δ_R 21.62 is assigned to a methyl group that is gauche to the lone pair and δ_W 10.71 to a methyl anti to the lone pair.[15] The major ^{1}H NMR subspectrum of **EMAP-d_7** (Figure 5; Table 3) also shows two well-separated isopropyl methyl signals. Again on the basis of established chemical shift trends, the resonance at δ_R 1.12 is assigned to a methyl group that is gauche to the lone pair and δ_Y 0.80 to a methyl anti to the lone pair.[12,14] *The isopropyl methine proton must be in the G or G' orientation.* For the conformation(s) associated with the major subspectrum, one isopropyl methyl group must be anti to the lone pair. This precludes the **AG** and **AG'** conformations in which the ethyl methyl group adopts an **A** orientation introducing seriously destabilizing *syn*-1,5-dimethyl repulsions. Therefore, the ethyl methyl group must be oriented gauche to the lone pair. The ^{1}H NMR spectrum of the methylene protons at 96 K shows a closely spaced DF spectrum (Figure 5; Table 3). In light of the fact that the chemical shift difference between NCH_2 protons that are oriented in positions anti and gauche to the lone pair is about 1 ppm, the closely spaced DF spectrum suggests strongly that a conformational exchange is still fast on the NMR chemical exchange time scale.[12,14] This is best rationalized in terms of rapid interconversion between **G'G'** and **GG'** conformations (Scheme 1; all conformations have S configuration at nitrogen). The **G'** orientation of the isopropyl methine proton allows interconversion between comparably populated **G'G'** and **GG'** conformations and also allows rapid averaging of the chemical shifts of the methylene protons via an isolated rotation process that is known to have a barrier too low to be DNMR-visible ($\Delta G^{\ddagger}$ < 4.5 kcal/mol).[12,14] During this process, the methyl group on the ethyl substituent passes the lone pair and each diastereotopic methylene proton exchanges between sites anti and gauche to the lone pair. The closely spaced DF spectrum reflects time-averaging of the methylene protons frequencies. Therefore, the major subspectrum is assigned to the **G'G'** and **GG'** conformations that undergo rapid exchange even at 95 K.

The second most intense ^{13}C NMR subspectrum (34%; Figure 2, Table 1) also shows two well-separated isopropyl methyl resonances at δ_M 21.97 and δ_V 12.08. The signal at δ_M 21.97 is assigned to a methyl group that is gauche to the lone pair and δ_V 12.08 to a methyl anti to the lone pair.[15] The corresponding ^{1}H NMR subspectrum of **EMAP-d_7** at 96 K (33%; Figure 5, Table 3) also shows two well-separated isopropyl methyl signals. The resonance at δ_S 1.12 is assigned

SCHEME 1: Stable Equilibrium Conformations of *N*-Ethyl-*N*-methyl-2−aminopropane (EMAP; S Configuration at Nitrogen)[a]

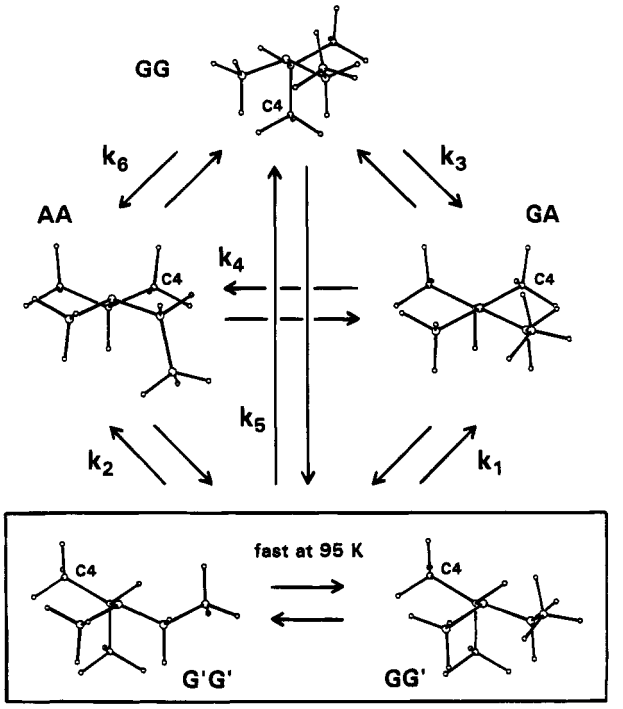

[a] Interconversion between the **G'G'** and **GG'** conformers is fast at 95 K. All other conformational exchanges in Scheme 1 have barriers high enough to be DNMR-detectable.

to a methyl group that is gauche to the lone pair and d_X 0.86 to a methyl anti to the lone pair.[12,14] *The isopropyl methine proton must be in the G or G' orientation.* Since one isopropyl methyl group must be anti to the lone pair, this precludes conformations that have the ethyl methyl group in the **A** orientation (*vide supra*). Therefore, the ethyl methyl group must be oriented gauche to the lone pair. The ^{1}H NMR subspectrum of the NCH_2 protons of **EMAP-d_7** at 96 K shows a widely spaced CM spectrum ($\Delta\delta$ 0.76; Figure 5, Table 3). In light of the fact that the chemical shift difference between NCH_2 protons that are oriented respectively anti and gauche to the lone pair is about 1 ppm, the widely spaced CM spectrum reveals a strong conformational preference of the ethyl group for the **G** or **G'** orientation and no time-averaging due to conformational exchange. The only conformation that is consistent with all the NMR data is the **GG** form (Scheme 1). In the **GG** conformation, the methine proton and the ethyl methyl group are in **G** orientations. The ethyl methyl group of the **GG** conformation (Scheme 1) is essentially "locked" in the **G** position. Any significant concentration of the **G'G** conformation is precluded by destabilizing *syn*-1,5-dimethyl repulsions. Time-

TABLE 5: Relative Free Energies of EMAP Conformations Determined by ^{13}C NMR Spectroscopy

conformer(s)	relative free energy (kcal/mol)[a]
G'G'/GG'	0.00
GG	0.10
AA	0.47
GA	0.64

[a] At 95 K.

averaging of the methylene protons chemical shifts via exchange between **GG** and **G'G** conformations is not possible. A strong preference of the ethyl group for the **G** orientation is consistent with the large difference between the chemical shifts of the diastereotopic methylene protons.

The third most intense ^{13}C NMR subspectrum (5%; Figure 2, Table 1) shows only one resonance for the isopropyl methyl carbons consistent with superposition of the resonances (δ_N 21.87 and δ_O 21.87) due to these two carbons. The chemical shift (δ 21.87) reveals that the isopropyl methyl groups are both gauche to the lone pair.[15] The corresponding ^1H NMR subspectrum of **EMAP-d_7** at 96 K (4%; Figure 5, Table 3) also shows only one resonance for the isopropyl signals consistent with the superposition of two signals at δ_V 1.07 and δ_W 1.07. The chemical shifts at δ 1.07 reveal isopropyl methyl groups that are both gauche to the lone pair.[12,14] *The isopropyl methine proton is in the A orientation.* A salient characteristic of this ^{13}C NMR subspectrum is the ethyl methyl chemical shift at δ_X 5.01 (Figure 2). This chemical shift is 8−9 ppm to lower frequency (higher field) than those for methyl groups that are gauche to the lone pair (Table 1) and reveals an ethyl methyl group that is anti to the lone pair.[15] The corresponding ^1H NMR subspectrum of **EMAP-d_7** at 96 K (4%; Figure 5, Table 3) shows a closely spaced AB spectrum for the methylene protons consistent with both protons being gauche to the lone pair and the ethyl methyl group being anti to the lone pair.[12,14] One is led inexorably to assign this subspectrum to the **AA** conformation (Scheme 1).

Having assigned three subspectra to the **GG'**, **G'G'**, **GG**, and **AA** conformations, the fourth subspectrum (2−3%) can be assigned by default. The only remaining stable equilibrium conformation that does not have *syn*-1,5-dimethyl repulsions is the **GA** form and this must be assigned to the least intense subspectrum (2−3%; Figures 2 and 5, Tables 1 and 3). Identical ^{13}C and ^1H chemical shifts for the isopropyl methyl groups at frequencies characteristic of methyl groups that are gauche to the lone pair are consistent with the **GA** conformation (Tables 1 and 3). The ^{13}C chemical shift of the ethyl methyl group reveals a methyl group that is gauche to the lone pair. While the low intensity of this subspectrum made it difficult to accurately place the chemical shifts of the methylene protons (Table 3), it was necessary to use a widely separated EN spectrum to achieve accurate fits of the DNMR spectra under conditions of slow and intermediate exchange. This is consistent with an ethyl methyl group that is "locked" in the **G** orientation.

The relative free energies of the stable, NMR-detectable **EMAP** conformations are compiled in Table 5.

Having assigned the four subspectra of **EMAP** to specific conformations (Scheme 1; Figures 2 and 5) and identified the preferred pathways for magnetization exchange, perusal of Tables 2 and 4 allows assignment of preferred conformational exchange pathways that involve isolated rotation about *N*-ethyl and *N*-isopropyl bonds. The NMR-detectable conformations of one enantiomer of **EMAP** (S configuration at nitrogen) are shown in Scheme 1. In Scheme 1, interconversion occurs via isolated rotation about carbon−nitrogen bonds. Interconversion between the **G'G'** and **GG'** forms within the box in Scheme 1 is fast on the DNMR time scale at 95 K (*vide supra*). All other conformational exchanges in Scheme 1 involve at least one C−CH_3/N−alkyl eclipsing and have barriers high enough to be DNMR-visible. Four conversions (k_1−k_4; Scheme 1) involve one C−CH_3/N−alkyl, one C−H/N−alkyl and one C−CH_3/N−LP or C−H/N−LP eclipsings. One other process (k_5; Scheme 1) has a barrier slightly larger and involves two C-CH_3/N-alkyl and one C-H/N-LP eclipsings. The k_6 conversion (Scheme 1) may have a barrier comparable to that for the k_5 process. The barrier to inversion−rotation at nitrogen ($\Delta G^{\ddagger}$ = 7.5 kcal/mol at 160 K) is at least 1.3 kcal/mol higher than all isolated rotation barriers (Tables 2 and 4).

CHART 1

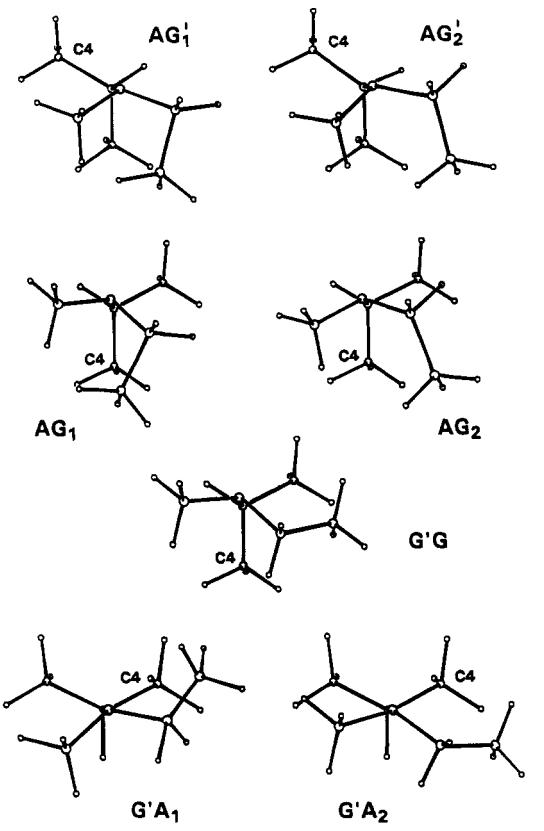

Molecular Mechanics Calculations

Molecular mechanics calculations done by using the Allinger−Profeta amine force field in the MM2(87) computer program agree with the NMR results and provide additional insight into the stereodynamics of **EMAP**.[17] A 5000-point optimized energy surface for **EMAP** was computed as a function of two dihedral angles. One dihedral angle (C4−C3−N1−LP) is associated with the isopropyl group. C4 is a methyl carbon on the isopropyl group. C4 is labeled on the NMR-detectable equilibrium conformers shown in Scheme 1 and on the substantially less stable, NMR-undetectable equilibrium conformations (**AG'$_1$**, **AG'$_2$**, **AG$_1$**, **AG$_2$**, **G'G**, **G'A$_1$**, **G'A$_2$**) shown in Chart 1. The other dihedral angle (C7−C6-N1−LP) is associated with the ethyl group. C7 is the methyl carbon on the ethyl group. The energy contour map is illustrated in Figure 6. The lower plot in Figure 6 is a two-dimensional representation of the energy surface that employs isoenergetic contour lines. The energy separation between the contours is set at 1.0 kcal/mol. Energy mimima correspond to specific equilibrium conformations for **EMAP**; these are labeled in bold black letters. Energy maxima, i.e., energy peaks or "mountain tops", are

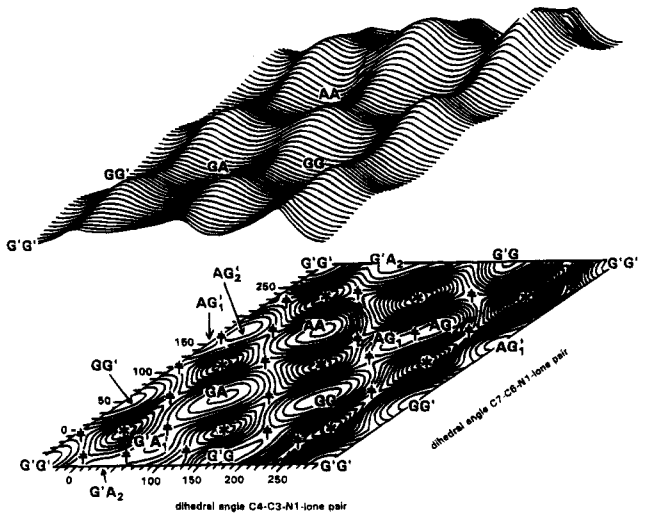

Figure 6. A 5000-point optimized energy contour map for *N*-ethyl-*N*-methyl-2-aminopropane (**EMAP**) computed as a function of two dihedral angles by using Allinger's MM2(87) computer program.[17] The dihedral angles are defined in the text. In the lower two-dimensional plot, the separation between the contour lines is 1.0 kcal/mol. An energy peak is indicated by an asterisk. A transition state is indicated by a double dagger. A pair of letters indicates an equilibrium conformation at an energy minimum. In the upper three-dimensional plot of the energy surface, only the equilibrium conformations present at concentrations high enough to be NMR-detectable are indicated.

TABLE 6: MM2(87) Relative Energies and Selected Dihedral Angles for the Equilibrium Conformations of EMAP

	dihedral angle (deg)		relative
conformer	C4−C3−N1-LP	C7−C6−N1-LP	energy (kcal/mol)
G′G′	−57	−61	0.0[a]
GG	181	57	0.13
GG′	−52	54	0.21
AA	63	183	0.39
GA	62	63	0.53
G′G	168	−58	2.69
AG_2	198	182	3.13
AG'_2	−32	184	3.18
AG'_1	−59	154	3.27
AG_1	175	157	3.30
$G'A_1$	63	−21	3.52
$G'A_2$	32	−60	4.29

[a] $\Delta H_f = -22.90$ kcal/mol.

labeled with asterisks (*), and saddle points are labeled with double daggers (‡). The upper plot is a three-dimensional representation of the energy surface. Only the NMR-detectable conformations are labeled on this surface.

Optimized MM2 calculations (Newton−Raphson minimization) in the region of each energy minimum predict the **G′G′** conformation (Scheme 1; $\Delta H_f = -22.90$ kcal/mol) to be the most stable. The C4−C3−N1−LP dihedral angle is −57°. The C7−C6−N1−LP dihedral angle is −61°. The **GG** form is computed to be only 0.13 kcal/mol higher in energy than **G′G′**. For the **GG** form, the C4−C3-N1-LP dihedral angle is 181° (Scheme 1). The C7−C6−N1−LP dihedral angle is 57°. Three other equilibrium conformations (Scheme 1; **GG′**, **AA**, **GA**) have energies within 0.53 kcal/mol of that for the **G′G′** form (Table 6). MM2(87) predicts that all five of these conformations will be present at concentrations high enough to be NMR-detectable. The relative energies and selected dihedral angles for all the equilibrium conformers of **EMAP** are compiled in Table 6. While the NMR spectra do not allow a direct measure of the relative energies of the **G′G′** and **GG′** conformations,

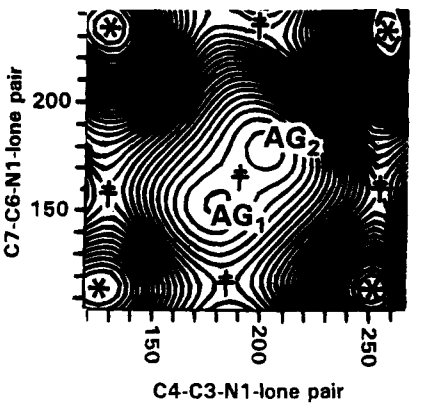

Figure 7. Section of the MM2(87) energy contour map that illustrates libration between the unstable **AG_1** and **AG_2** conformations.[17] The separation between contours is 0.5 kcal/mol.

the agreement between the relative energies determined by NMR (Table 5) and calculated by the MM2(87) force field is excellent.

In light of the excellent agreement between the relative conformational energies determined by NMR and those computed by MM2(87), it is reasonable to assume that MM2(87) will give useful insight into the stereodynamics of high energy NMR-undetectable equilibrium conformations of **EMAP**. Those equilibrium geometries that have destabilizing *syn*-1,5-dimethyl interactions between the ethyl methyl group and an isopropyl methyl group, such as the **AG_1** and **AG_2** forms are computed to be 3.30 and 3.13 kcal/mol, respectively, higher in energy than the **G′G′** form. The MM2(87) energy surface suggests that the **AG_1** and **AG_2** conformations interconvert via a low barrier libration process ($\Delta H^{\ddagger} < 1$ kcal/mol) involving low-amplitude torsions about the N−CH and N−CH_2 bonds and close passage of *syn*-1,5-methyl groups in the transition state. A section of the two-dimensional energy surface that encompasses the **AG_1** and **AG_2** conformations is shown in Figure 7. The separation between the energy contours in Figure 7 is 0.5 kcal/mol. The energy surface calculations predict analogous stereodynamics for the **AG'_1** and **AG'_2** conformations, and for the **$G'A_1$** and **$G'A_2$** forms (Figure 6). Starting from the **G′G** conformation, the surface calculation also predicts that a counterclockwise torsion about the CH_2−N bond does not result in another **G′G** equilibrium geometry but does result in a continuous increase in energy along a valley toward the transition state for conversion to the stable **GG** conformation.

The major NMR subspectrum (Figures 2 and 5) is best rationalized in terms of comparably populated **G′G′** and **GG′** conformations that exchange rapidly even at 95 K (*vide supra*). The **G′G′** and **GG′** conformers interconvert directly (Scheme 1) via an itinerary that involves the ethyl methyl group passing the lone pair and C-H bonds passing N-C bonds. By using a general dihedral angle driver calculation, the MM2(87) barrier for this isolated rotation process is calculated to be 4.4 kcal/mol. This barrier is identical to that calculated for an analogous interconversion in diethylmethylamine.[12] The major ^{1}H DNMR subspectrum of **EMAP-d_7** at 96 K suggests that the actual rotation barrier may be lower than 4.4 kcal/mol (*vide supra*). The calculated value is below the lower limit for DNMR detection in our laboratory (4.5 kcal/mol).[15] MM2(87) predicts that the population ratio of **G′G′** to **GG′** forms to be about 3 to 1 at 95 K. Rapid exchange between such comparably populated **G′G′** and **GG′** species would produce the time-averaged character of the major subspectrum and is rigorously consistent with the rationale used to assign the major subspectrum (*vide supra*).

TABLE 7: MM2(87)-Calculated Isolated Rotation Barriers in EMAP

conformational exchange process[a]	barrier (kcal/mol)
G'G' to **GG'**	4.4[b]
GA to **AA**	5.6[b]
GG' to **GA**	5.4[c]
GG to **GA**	5.5[c]
GG to **GG'**	8.5[c]

[a] See Scheme 1. [b] Rotation about the N−CH_2 bond. [c] Rotation about the N−CH bond.

In contrast, the MM2(87)-calculated barrier for the **GG** to **GA** process (Scheme 1; k_3) during which an isopropyl methyl group passes ethyl is 5.5 kcal/mol and is predicted correctly to be high enough to be DNMR-visible. Additional MM2(87)-calculated isolated rotation barriers are compiled in Table 7. If rotation about the N−CH_2 or N−CH bond involves at least one C-CH_3/N-alkyl eclipsing, these processes are predicted to have have barriers high enough to be DNMR-visible. Except for interconversion of the **G'G'** and **GG'** conformations, all other conformational exchanges between the NMR-detectable conformations in Scheme 1 are predicted to have barriers high enough to be DNMR-visible. This is rigorously consistent with the conformational exchange kinetics derived from simulations of the DNMR spectra (*vide supra*). In fact, a comparison of the experimentally determined rotation barriers ($\Delta G^{\ddagger}$ values) in Tables 2 and 4 with the MM2(87) barriers (Table 7, $\Delta H^{\ddagger}$ values) shows excellent agreement except for the **GG** to **GG'** conversion. Similar observations have been made regarding the stereodynamics of isopropyldimethylamine.[15]

Conformational preferences in **EMAP** determined by NMR spectroscopy (Table 5) and predicted by molecular mechanics (Table 6) are in excellent agreement. Those conformations of **EMAP** that have one isopropyl methyl group anti and the other gauche to the lone pair are dominant (relative $\Delta G°$ values = 0.0−0.1 kcal/mol) over those that have both isopropyl methyl groups gauche to the lone pair (relative $\Delta G°$ values = 0.5−0.6 kcal/mol). This is in some contrast to isopropyldimethylamine in which there is essentially a statistical distribution of conformational populations among the three isopropyl group rotamers.[15] There is a free energy preference of 0.070 kcal/mol at 94 K for that conformation of isopropyldimethylamine that has one isopropyl methyl group anti and the other gauche to the lone pair over that conformation with both isopropyl methyls gauche to the lone pair. A flattening of the nitrogen pyramid in **EMAP** would lead to enhanced eclipsing and increased repulsions between vicinal substituents in the **AA** and **GA** conformers and destabilization. However, a comparison of MM2(87)-calculated CNC bond angles in isopropyldimethylamine and **EMAP** suggests virtually no difference in pyramidality at nitrogen. Since a decrease in pyramidality at nitrogen in **EMAP** as compared to isopropyldimethylamine is not predicted by the MM2(87) force field, it is apparent that optimizing nonbonded repulsions between the isopropyl and ethyl groups is best accomplished by an anti/gauche orientation of the two isopropyl methyl groups. Analogous conformational preferences are observed for *N*-ethyl-*N*-methyl-2-aminobutane.[14]

Experimental Section

NMR Spectra. The NMR spectra were recorded by using a Bruker WM-250 NMR system at the University of Vermont (^{13}C spectra) and a Bruker WP-270 NMR system at the Northeast Regional NMR Facility at Yale University (^1H spectra). The WM-250 magnet pole gap was modified to allow safe operation (no magnet O-ring freezing) down to 93 K. NMR sample temperature was varied by using a custom-built cold nitrogen gas delivery system used in conjunction with the Bruker BVT-1000 temperature control unit. Temperature measurement is accurate to ±3 K. NMR samples were prepared in precision 5- or 10-mm tubes and sealed after four freeze−pump−thaw cycles. All spectra are referenced to tetramethylsilane at 0 ppm.

***N*-Ethyl-*N*-methyl-2-aminopropane (EMAP).** Acetone (16.0 g, 0.27 mol), methylamine hydrochloride (32.0 g, 0.47 mol), and methanol (150 mL) were placed in a three-neck round bottom flask equipped with an efficient condenser. The mixture was stirred over an ice-water bath while sodium cyanoborohydride (15.2 g, 0.24 mol) was added slowly. The mixture was stirred at room temperature for 72 h. With cooling, concentrated HCl (30 mL) was added until the pH of the mixture was less than 2. The liquid was removed under vacuum. Water (20 mL) was added to the resulting white residue. The aqueous solution was washed with four 50-mL portions of ether. The aqueous solution was placed in a 3-neck round bottom flask equipped with an efficient condenser and stirred over an ice bath while solid KOH (40 g) was added to pH > 10. A thick white slurry resulted. NaCl (20 g) and ether (40 mL) was added to the slurry. The mixture was tightly stoppered and stirred at room temperature for 24 h. The ether layer was separated and dried over anhydrous Na_2SO_4 for 12 h. The presence of *N*-methyl-2-aminopropane in the ether solution was confirmed by ^1H NMR. The solution of *N*-methyl-2−aminopropane in ether was dried over molecular sieves for 24 h. The amine solution was placed in a in a three-neck round-bottom flask fitted with an efficient condenser equipped with a drying tube. The solution was stirred over an ice bath while acetyl chloride (5 g, 0.06 mol) was added dropwise. The mixture was then refluxed for 5 h and NaOH (8 g) added with cooling. The mixture was stirred at room temperature for 12 h and filtered, and the ether removed by using a rotary evaporator. The liquid residue was vacuum distilled through a Vigreux column. The resulting isopropylmethylacetamide was confirmed by ^1H NMR. A portion of the isopropylmethylacetamide (2 g, 0.0173 mol) in ether (20 mL) was dried over molecular sieves for 24 h. The dry amide solution was placed in a three-neck round-bottom flask fitted with an efficient condenser equipped with a drying tube and stirred over an ice bath while 1 M ethereal lithium aluminum hydride (17.5 mL, 0.0175 mol) was added dropwise. The resulting mixture was refluxed for 5 h. The reaction mixture was stirred over an ice bath while an aqueous 15% NaOH solution (4 mL) was added. The resulting mixture was filtered and the ether solution dried over Na_2SO_4 for 1 h. The bulk of the ether was removed by distillation through a Vigreux column under 1 atm of nitrogen. *N*-Ethyl-*N*-methyl-2−aminopropane was purified by using a 25% SF-96/5% XE-60 on Chromosorb WAW GLPC column (20 ft x 3/8 in.) at 373 K. The structure was confirmed by ^1H NMR (CCl_4, 298 K) δ_A 2.74 (1H, septet, CH), δ_D 2.28 (2H, quartet, CH_2), δ_M 2.08 (3H, singlet, NCH_3), δ_X 0.99 (3H, triplet, ethyl CH_3, $^3J_{DX}$ = 7.2 Hz), δ_Y 0.94 (6H, doublet, $C(CH_3)_2$), $^3J_{AY}$ = 6.4 Hz), ^{13}C NMR (see text), and mass spectroscopy *m/e* (M^+): 101.

***N*-(Ethyl-2,2,2-d_3)-*N*-(methyl-d_3)-2-aminopropane-2-*d* (EMAP-d_7).** With stirring and cooling under N_2, acetone (36 g, 0.56 mol) in 40 mL of anhydrous ether was added dropwise to $LiAlD_4$ (6 g, 0.14 mol) in anhydrous ether (80 mL). The mixture was allowed to reflux for 2 h under an efficient condenser equipped with a drying tube. With cooling and stirring, water (10 g) was added dropwise and refluxing continued for an additional 2 h. The resulting white precipitate was removed by filtration. The resulting solution was distilled on a spinning band column to give 13.4 g of $CH_3CD(OH)CH_3$

(bp 81−83 °C). With cooling and stirring, fuming H_2SO_4 (20 g) was slowly added to 24 mL of 48% HBr. $CH_3CD(OH)CH_3$ (13.4 g, 0.2 mol) was then added to the acid solution. The reaction mixture was stirred at room temperature for 0.5 h. The product was distilled from the reaction vessel via a short-path column, washed with 30 mL of cold dilute aqueous $NaHSO_3$, 50 mL of cold concentrated HCl, 50 mL of water, and 50 mL of 10% aqueous $NaHCO_3$, and dried over calcium chloride. Purification was done by distillation on a spinning band column to give 15 g of $CH_3CDBrCH_3$ (bp 60 °C). $CH_3CDBrCH_3$ (26 g, 0.21 mol) was added to potassium phthalimide (46.3 g, 0.25 mol) in 135 mL of dimethylformamide under N_2. The mixture was stirred for 42 days. Water (100 mL) and chloroform (50 mL) were added to the reaction mixture. The bottom chloroform layer was separated, and the water layer was washed with two 30-mL portions of chloroform. All chloroform extracts were combined and washed with one 65-mL portion of 0.1 M NaOH solution. After the chloroform was removed under vacuum, the solid residue was washed with cold water to yield 37.6 g of white, crystalline *N*-(isopropyl-2*d*)-phthalimide. Hydrazine (95%; 6.6 g, 0.2 mol) was added to *N*-(isopropyl-2*d*)-phthalimide (37.6 g, 0.2 mol) in 310 mL of ethanol. The mixture was stirred for 64 h. With cooling at 0 °C and stirring, HCl (37%; 22 mL) was added slowly. The mixture was stirred for 2 h, the solid was removed by filtration and washed with 120 mL of ethanol to yield 28 g of phthalhydrazide (90%). The ethanol filtrate and washes were combined. The ethanol was removed under vacuum to yield 16.8 g of crystalline amine hydrochloride. To a cooled, stirred solution of 12 g (0.12 mol) of amine hydrochloride in 50 mL of water and 50 mL of ether was added slowly 6.9 g (0.12 mol) of KOH in 10 mL of water. The ether and water layers were separated. The ether solution of the amine was added to ethyl-2,2,2-d_3-iodide (10 g, 0.06 mol) in 50 mL of ether and stirred for 5 h. Gaseous HCl was bubbled through the solution and the ether removed under vacuum yielding solid amine hydrochloride. To a stirred and cooled mixture of amine hydrochloride (2.6 g; 0.03 mol) in 10 mL of water and 20 mL of ether was added slowly 1.7 g of KOH in 5 mL of water. The ether and water layers were separated. The ether solution of the amine was added dropwise to 3.8 g (0.03 mol) of methyl-d_3 iodide in 20 mL ether. After refluxing for 2 h, gaseous HCl was bubbled through the ether solution. The resulting solid amine hydrochloride was isolated by filtration and dissolved in 20 mL of water. Solid KOH was added to saturation. The amine was extracted with three 20-mL portions of ether. The ether extracts were dried (Na_2SO_4) and filtered, and most of the ether removed on a spinning band column. *N*-(Ethyl-2,2,2-d_3)-*N*-(methyl-d_3)-2-aminopropane-2*d* was purified on a 20% SE-30 Chromosorb W GLPC column. The structure was confirmed by ^1H NMR (see text).

Acknowledgment. We are grateful to the University of Vermont Academic Computing Center for excellent computational support.

References and Notes

(1) Bushweller, C. H. In *Acyclic Organonitrogen Stereodynamics*; Lambert, J. B. Takeuchi, Y., Eds.; VCH Publishers: New York, 1992.

(2) Bushweller, C. H.; Anderson, W. G.; Stevenson, P. E.; O'Neil, J. W. *J. Am. Chem. Soc.* **1975**, *97*, 4338. Bushweller, C. H.; Anderson, W. G.; Stevenson, P. E.; Burkey, D. L.; O'Neil, J. W. *J. Am. Chem. Soc.* **1974**, *96*, 3892.

(3) Tsuboi, M.; Hirakawa, A. Y.; Tamagake, K. *J. Mol. Spectrosc.* **1967**, *22*, 272. Nishikawa, T.; Itoh, T.; Shimoda, K. *J. Am. Chem. Soc.* **1977**, *99*, 5570. Wollrab, J. W.; Laurie, V. W. *J. Chem. Phys.* **1968**, *48*, 5058. Erlandson, G.; Gurdy, W. *Phys. Rev.* **1957**, *10*, 513. Lide, D. R., Jr.; Mann, D. E. *J. Chem. Phys.* **1958**, *28*, 572.

(4) Durig, J. R.; Li, Y. S. *J. Chem. Phys.* **1975**, *63*, 4110. Tsuboi, M.; Tamagake, K.; Hirakawa, A. Y.; Yamaguchi, J.; Nakagava, H.; Manocha, A. S.; Tuazon, E. C.; Fateley, W. G. *J. Chem. Phys.* **1975**, *63*, 5177.

(5) Krueger, P. J.; Jan, J. *Can. J. Chem.* **1970**, *48*, 3229.

(6) Durig, J. R.; Compton, D. A. C. *J. Phys. Chem.* **1979**, *83*, 2873.

(7) Durig, J. R.; Cox, F. O. *J. Mol. Struct.* **1982**, *95*, 85.

(8) Swalen, J. D.; Ibers, J. A. *Chem. Phys.* **1962**, *36*, 1914.

(9) Tsuboi, M.; Hirakawa, A. Y.; Takamitsu, I.; Sasaki, T.; Tamagake, K. J. *J. Chem. Phys.* **1964**, *41*, 2721. Tsuboi, M.; Hirakawa, A. Y.; Tamagake, K. *J. Mol. Spectrosc.* **1967**, *22*, 272.

(10) Wollrab, J. E.; Laurie, V. W. *J. Chem. Phys.* **1968**, *48*, 5058.

(11) Weston, R. E., Jr. *J. Am. Chem. Soc.* **1954**, *76*, 2645.

(12) Bushweller, C. H.; Fleischman, S. H.; Grady, G. L.; McGoff, P.; Rithner, C. D.; Whalon, M. R.; Brennan, J. G.; Marcantonio, R. P.; Domingue, R. P. *J. Am. Chem. Soc.* **1982**, *104*, 6224.

(13) Fleischman, S. H.; Whalon, M. R.; Rithner, C. D.; Grady, G. L.; Bushweller, C. H. *Tetrahedron Lett.* **1982**, 4233.

(14) Danehey, C. T., Jr.; Grady, G. L.; Bonneau, P. R.; Bushweller, C. H. *J. Am. Chem. Soc.* **1988**, *110*, 7269.

(15) Brown, J. H.; Bushweller, C. H. *J. Am. Chem. Soc.* **1992**, *114*, 8153.

(16) Bushweller, C. H.; Wang, C. Y.; Reny, J.; Lourandos, M. Z. *J. Am. Chem. Soc.* **1977**, *99*, 3938.

(17) Allinger, N. L. *QCPE*, 1987, Program No. MM2(87). Also see: Profeta, S., Jr.; Allinger, N. L. *J. Am. Chem. Soc.* **1985**, *107*, 1907. Schmitz, L. R.; Allinger, N. L. *J. Am. Chem. Soc.* **1990**, *112*, 8307. For a program to plot the two-dimensional energy contour map, see: Brown, J. H. *QCPE*, 1993, Program No. QCMP 126.

(18) Brown, J. H.; Bushweller, C. H. *QCPE*, 1993, Program No. 633. For a PC-based program to plot the DNMR spectra, see: Brown, J. H. *QCPE*, 1993, Program No. QCMP 123.